PRECLINICAL AND CLINICAL SPECTROSCOPY – Note

Magnetic Resonance in Medicine 71:1231–1237 (2014)

Intervertebral Disc Internal Deformation Measured by Displacements Under Applied Loading with MRI at 3T

Deva D. Chan and Corey P. Neu*

Purpose: Noninvasive assessment of tissue mechanical behavior could enable insights into tissue function in healthy and diseased conditions and permit the development of effective tissue repair treatments. Measurement of displacements under applied loading with MRI (dualMRI) has the potential for such biomechanical characterization on a clinical MRI system.
Methods: dualMRI was translated from high-field research systems to a 3T clinical system. Precision was calculated using repeated tests of a silicone phantom. dualMRI was demonstrated by visualizing displacements and strains in an intervertebral disc and compared to T_2 measured during cyclic loading.
Results: The displacement and strain precisions were 24 μm and 0.3% strain, respectively, under the imaging parameters used in this study. Displacements and strains were measured within the intervertebral disc, but no correlations were found with the T_2 values.
Conclusion: The translation of dualMRI to a 3T system unveils the potential for in vivo studies in a myriad of tissue and organ systems. Because of the importance of mechanical behavior to the function of a variety of tissues, it's expected that dualMRI implemented on a clinical system will be a powerful tool in assessing the interlinked roles of structure, mechanics, and function in both healthy and diseased tissues. **Magn Reson Med 71:1231–1237, 2014. © 2013 Wiley Periodicals, Inc.**

Key words: displacement; strain; intervertebral disc; elastography; clinical magnetic resonance imaging

The mechanical behavior of a biomaterial is intimately linked to its function, both within natural tissues and biocompatible materials. The material properties and also the loading environment affect the mechanical behavior of tissues, particularly as they relate to healthy and pathological conditions within the body. Noninvasive methods to quantify the mechanical behavior of biomaterials and tissues would permit the measurement of material properties while both preserving the native loading environment and accounting for its influence. Such methods would improve longitudinal studies in animals or humans, greatly reducing the number of animals or human subjects needed for clinical trials, among other benefits. Additionally, these methods could also be implemented to assess tissue quality in patients and monitor the long-term effectiveness of pharmacological or tissue engineering treatments. Some studies have attempted to correlate various relaxometry measures, such as T_2 and $T_{1\rho}$, to mechanical properties in a number of tissues (1,2), motivated by the idea that relaxometry measures correspond to biochemistry and, in turn, are related to mechanical behavior. However, these correlations are based on mechanical tests performed on explanted tissue and do not take advantage of the noninvasive nature of MRI to fully assess tissues within their native environment. Because techniques like displacement-encoded MRI can measure displacements and strains noninvasively (3), such a technique for biomechanical characterization of tissue could complement other quantitative MRI techniques (4) for the overall assessment of soft tissue function.

The goal of this study was to translate a noninvasive imaging technique that can measure displacements under applied loading with MRI (dualMRI) to a clinical 3T MRI system. Previous efforts in our lab have utilized dualMRI on a high-field MRI scanner, where displacements and strains were measured in explants of healthy cartilage (3) and in intact joints, including tibiofemoral cartilage (5) and degenerated intervertebral discs in animal models (6). Despite the advantages proffered by the higher magnetic field of research MRI systems, these systems are often limited to small volumes and are not approved for clinical use on human subjects. Translation of the dualMRI technique to a clinical scanner would allow for studies of live animals and human subjects, as well as larger tissues and biomaterials that would not be able to fit into the limited confines of a small-bore high-field MRI system. The technical challenge of implementing dualMRI on a living animal or human subject is twofold: (1) the translation of a load-synchronized, displacement-encoded MRI sequence and (2) the development of noninvasive, organ- or joint-specific loading systems capable of repeatable cyclic loading of the tissues of interest.

In this article, to address the first of these challenges, we report the translation of dualMRI to a clinical MRI system at 3T, the determination of technique precision using imaging phantoms, and the demonstration of this technique within an intact human intervertebral disc section. We also demonstrate that the displacements and strains measured with dualMRI can be compared to the T_2 distribution of the disc measured under cyclic load.

Weldon School of Biomedical Engineering, College of Engineering, Purdue University, West Lafayette, Indiana, USA.

Grant sponsor: National Science Foundation; Grant number: CMMI 1100554; Grant sponsors: James V. Stack Fellowship and Purdue MRI Facility.

*Correspondence to: Corey P. Neu, Ph.D., Weldon School of Biomedical Engineering, Purdue University, West Lafayette, IN. E-mail: cpneu@purdue.edu

Received 7 December 2012; revised 15 March 2013; accepted 18 March 2013

DOI 10.1002/mrm.24757
Published online 6 May 2013 in Wiley Online Library (wileyonlinelibrary.com).

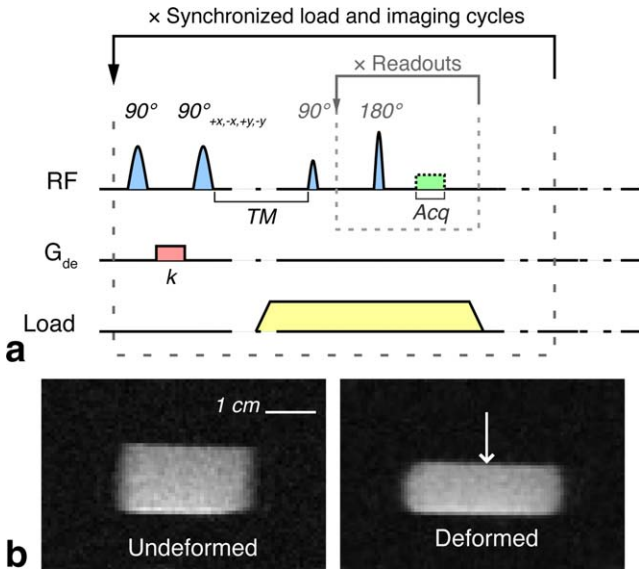

FIG. 1. Timing of dualMRI on a 3T MRI system. This schematic shows the timing events for dualMRI in a clinical 3T MRI system (**a**). Cyclic loading was synchronized with radiofrequency (RF) pulses and gradient actions, including the gradient applied for displacement encoding (G_{de}). Gradient actions in the readout, phase-encode, and slice-select directions are typical for a single-shot fast spin echo (SSFSE) acquisition and, for brevity, are not shown here. RF transmission pulses are shown in the solid lines and receive action (i.e. acquisition) is shown in dashed lines. Standard MRI scans of an undeformed and deformed imaging phantom (**b**) are also shown to demonstrate the time points during which the key dualMRI actions were performed. The undeformed image was acquired during the equivalent time point when the phase-cycled RF pulses and displacement encoding gradient, with gradient strength *k*, were applied. After a mixing time (TM), dualMRI data was acquired using SSFSE during the deformed state.

This research represents a critical step toward the noninvasive in vivo measurement of biomaterial mechanical properties, permitting future studies in clinical and animal research.

METHODS

Displacement-Encoded Imaging

dualMRI was implemented on a 3T clinical MRI system (General Electric Signa HDx, Waukesha, WI) using an eight-channel knee volume coil and a custom pulse sequence (Fig. 1). Spatial modulation of magnetization (7) was implemented with two 90° radiofrequency (RF) pulses, the second of which was phase cycled for cosine and sine modulation to eliminate artifacts [CANSEL, (8)]. A directional magnetic gradient was applied between the two 90° RF pulses to label the phase according to the initial configuration of the tissue of interest. To capture in-plane displacements, displacement encoding was applied in the direction of loading (*y*) as well as the direction transverse to loading (*x*). Subsequent imaging with a single-shot fast spin echo (SSFSE) technique during the load plateau was then used to acquire a single-slice, displacement-encoded image of the deformed configuration of the tissue of interest.

After complementary phase-cycled scans were combined for CANSEL (8), a phase difference reconstruction across all channels (9) was used to isolate the overall phase difference between the reference and encoded scans. A sum of squares magnitude reconstruction across all channels was used to compute the signal-to-noise ratio (SNR) of a region-of-interest (ROI) with respect to a region of noise (i.e., air). The displacement in the encoding direction was then computed as a function of the phase difference, as previously described (3,10). Orthogonal in-plane displacements were then smoothed with a Gaussian 5 × 5 kernel (11) prior to estimation of the Green-Lagrange strain tensor (12).

Precision of dualMRI

The precision of our dualMRI technique was evaluated across five repeated scan series of a silicone gel phantom (Sylgard 527, Dow Corning, Elizabethtown, KY) that was cyclically loaded with an MRI-compatible loading apparatus (4). Displacement encoding was accomplished with an encoding gradient area of 3.9145 mT μs/mm, equivalent to displacement encoding of 0.33 π/mm, based on pilot studies that showed no more than ±3 mm of expected internal deformation. A mixing time (TM) of 600 ms, which included spoiler gradients immediately before acquisition, allowed for the onset of loading prior to data acquisition during the load plateau. TM is limited by the capabilities of the load apparatus (i.e., time required to reach desired load); therefore, the minimum TM allowable by the loading system was chosen to maximize the stimulated echo signal. SSFSE acquisition parameters were as follows: effective echo time (TE) = 62 ms, matrix size = 256 × 256, spatial resolution = 703 × 703 μm^2, and eight averages. The SSFSE sequence was limited by the system software to a field of view of 180 × 180 mm^2 and slice thickness of 3 mm. Because the acquisition and the loading were synchronized, the effective repetition time was dictated by the 3-s duration loading cycles, during which a load of 18.5 N was applied for 1.5 s, based on previous studies (4,6). The experiment time for all scans within each repeated dualMRI experiment was 10 min. Image acquisition was completed before the load was released within each cycle. Imaging data was processed as described above to calculate in-plane displacements. Precision was computed as the pooled standard deviation across the five repeated scan series of displacement and strain values across 16 points within the imaging phantom (3,5). Precision was calculated for raw displacements and displacements and strains after 10–100 cycles of smoothing (11).

dualMRI in an Intact Intervertebral Disc Section

To demonstrate the dualMRI technique in a biological specimen, cyclic compression and imaging of a cadaveric intervertebral disc section was synchronized. A cadaveric lumbar spine was obtained from a tissue bank (AlloSource, Centennial, CO) and kept frozen until specimen preparation. The donor was a 22-year-old male and weighed 111 kg, with no medical history of disc degeneration or other spine disease. A spine segment inclusive of the fourth lumbar vertebra (L4) to the fifth lumbar

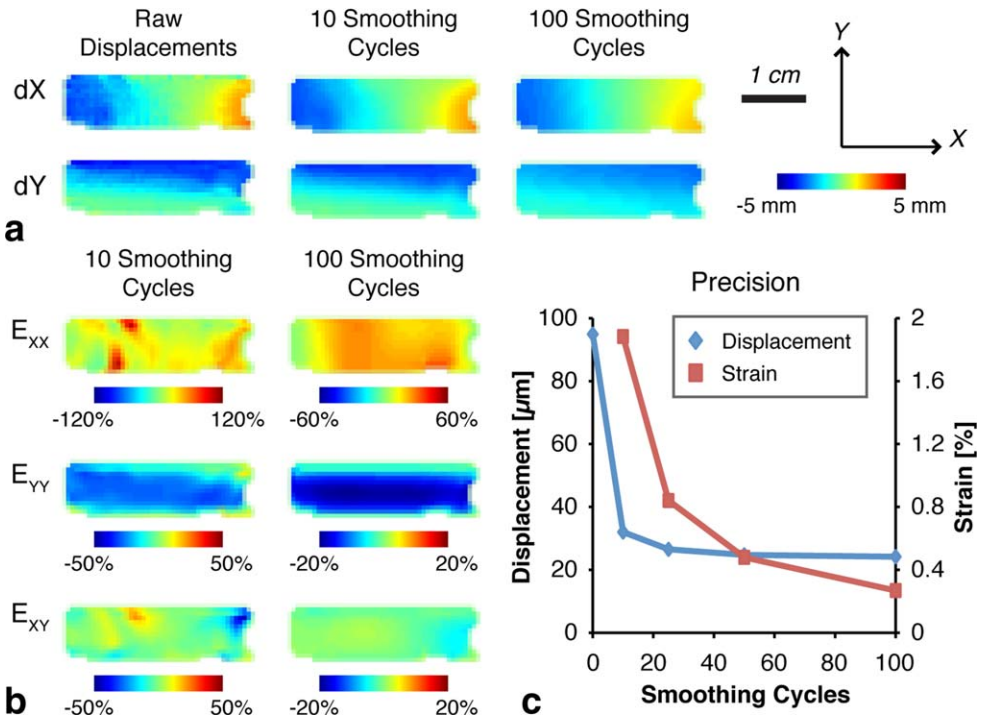

FIG. 2. Displacement and strains in a silicone phantom used to evaluate precision. A cyclically loaded silicone phantom was used to validate displacements (**a**) and strains (**b**), and determine relationships between displacement and strain precision (**c**). Including raw displacements, and displacements and strains after 10 and 100 smoothing cycles, depict the influence of displacement smoothing on deformation patterns. Displacements and strains were measured with dualMRI under the same loading conditions that resulted in the undeformed and deformed images in Figure 1B.

vertebra (L5) was excised. The spinal processes and facet joints were removed by transecting the pedicles of the vertebral arch, retaining the vertebral bodies superior and inferior to the L4/L5 intervertebral disc. The L4 and L5 vertebral bodies were partially embedded in polymethylmethacrylate, permitting the full disc segment to be anchored into an MRI-compatible loading apparatus for cyclic compression.

Prior to cyclic loading, standard MRI was performed to obtain morphological data. Compression of 450 N was then applied with the MRI-compatible cyclic loading apparatus for 1.5 s during a 3-s cycle. Preconditioning of more than 500 loading cycles (based on pilot studies) was applied prior to dualMRI to ensure that the specimen reached a quasi-steady state deformation response to the cyclic loading (13). Displacement-encoded images were acquired during the load plateau period under quasi-steady state. Parameters for dualMRI were same as for the precision studies above. Displacements within the L4/L5 disc were smoothed to 100 smoothing cycles, and strains were computed. During cyclic loading, standard MRI images were also acquired in the undeformed and deformed configurations for the measurement of nominal change in height and width under cyclic compression. The total experiment time for all dualMRI scans was 20 min, excluding the time necessary for the specimen to achieve quasi-steady state (less than 20 min under this experimental loading regime).

T_2 Analysis

In addition, to investigate whether any correspondence existed between the presence of mechanical loading and mechanical behavior and the measured T_2, a known correlate to disc biochemistry (14) and stage of degeneration (15), we estimated T_2 prior to cyclic loading, during cyclic loading immediately after dualMRI, and immediately after the cessation of cyclic loading. T_2 was estimated using a set of fast spin echo acquisitions with variable TE (TEs = 20, 60, 100, 140, 180, and 240 ms) of the same imaging plane as dualMRI. Repetition time was set to 3000 ms, which is approximately four to five times T_1 of human disc (16), to minimize T_1-weighting. An electronic trigger was used to synchronize the acquisitions for T_2 mapping under cyclic loading. T_2 mapping experiments were performed within 10 min under each loading condition. A least squares fit of an exponential decay curve was used to estimate T_2 at each pixel within the disc ROI before, during and after cyclic loading. Histograms of the T_2 values in each ROI were generated using bins of 5 ms intervals for qualitative comparison. The ROIs were also divided into five regions along the width of the disc, and, separately, into five regions along the height of the disc. Average regional T_2 was computed and compared for each of these sections between loading conditions. Average T_2 values are reported as mean ± standard deviation. T_2 values were correlated pixel-by-pixel to displacements and strains using linear regression. Statistical significance was defined as $P < 0.05$.

RESULTS

dualMRI Precision

Displacements measured by dualMRI, displacements after smoothing, and estimated strains were visualized in the silicone phantom (Fig. 2). Over five repeated tests, the average SNR was 4.2, and the precision of raw displacements was 95 μm. After smoothing, the precision improved to 32 μm at 10 smoothing cycles and 24 μm at 100 smoothing cycles. Strain precision was 1.9% after 10 smoothing cycles but improved to 0.3% with 100 cycles of smoothing.

Intervertebral Disc Displacements and Strains

dualMRI on a 3T MRI system permitted the visualization of displacements and strains within the L4/L5 intervertebral disc (Fig. 3). The average SNR of the displacement-encoded images was 14.8. During cyclic loading, the height of the undeformed disc measured 12.7 mm, and the width was 57.6 mm. The height and width of the deformed disc during cyclic loading was 12.0 and 58.4 mm, respectively. Displacements measured with dualMRI were smoothed for strain calculations and ranged −1.25 to −0.85 mm in the loading direction and −0.26 to 0.67 mm in the direction transverse to loading. Strain in the loading direction ranged from −4.5 to 0.2%, while the nominal strain, as measured from images taken before and during loading, was −5.9%. Strains transverse to the loading direction ranged −2.2 to 4.4%, compared to 1.2% nominal strain. Shear strains ranged from −1.4 to 1.0%.

T_2 Values

The average T_2 values across the full disc before, during, and after cyclic loading were 76.8 ± 33.7, 80.8 ± 33.8, and 80.5 ± 34.7 ms, respectively (Fig. 4). Dividing the disc into width-wise and height-wise regions allowed for a visualization of the T_2 trends throughout the disc (Fig. 4b,c). Examination of the histogram of T_2 values and the T_2 maps did not show qualitative differences in the distribution of T_2 values among the before, during, and after cyclic loading conditions (Fig. 4d). Additionally, no significant correlations were found in any of the relationships between T_2 and raw displacement or between T_2 and displacements and strains after smoothing (Fig. 4e).

DISCUSSION

Translation of dualMRI from research (9.4 T/30 cm bore) to clinical (3.0 T/60 cm bore) MRI systems presented several technical challenges associated with the larger imaging volume and weaker magnetic field, including reduced spatial resolution and faster T_1 decay of the displacement-encoded signal. Despite a reduction in spatial resolution and increased slice thickness, the precision of raw displacement measurement, 95 μm, fell within the ranges of raw displacement precisions measured previously on a research MRI system (4,5). This is most likely because the precision of displacement is tied closely to the SNR (4), which is increased with larger voxel sizes. The displacement and strain fields and precision values after smoothing were also comparable to previous studies (Fig. 2). Precisions were measured in a linearly elastic and nonbiologic phantom to encompass the error inherent to the imaging side of the experiments and image processing while excluding any biological variability. It is important to note that desiccation, enzymatic degradation, and other time-dependent phenomena could affect the mechanical behavior of a biological tissue, which must be cyclically loaded and imaged across multiple repeated experiments for precision analysis. In addition, previous studies have shown that there is no significant bias in the measurement of displacement and estimation of strain (3), where bias was measured as the deviation

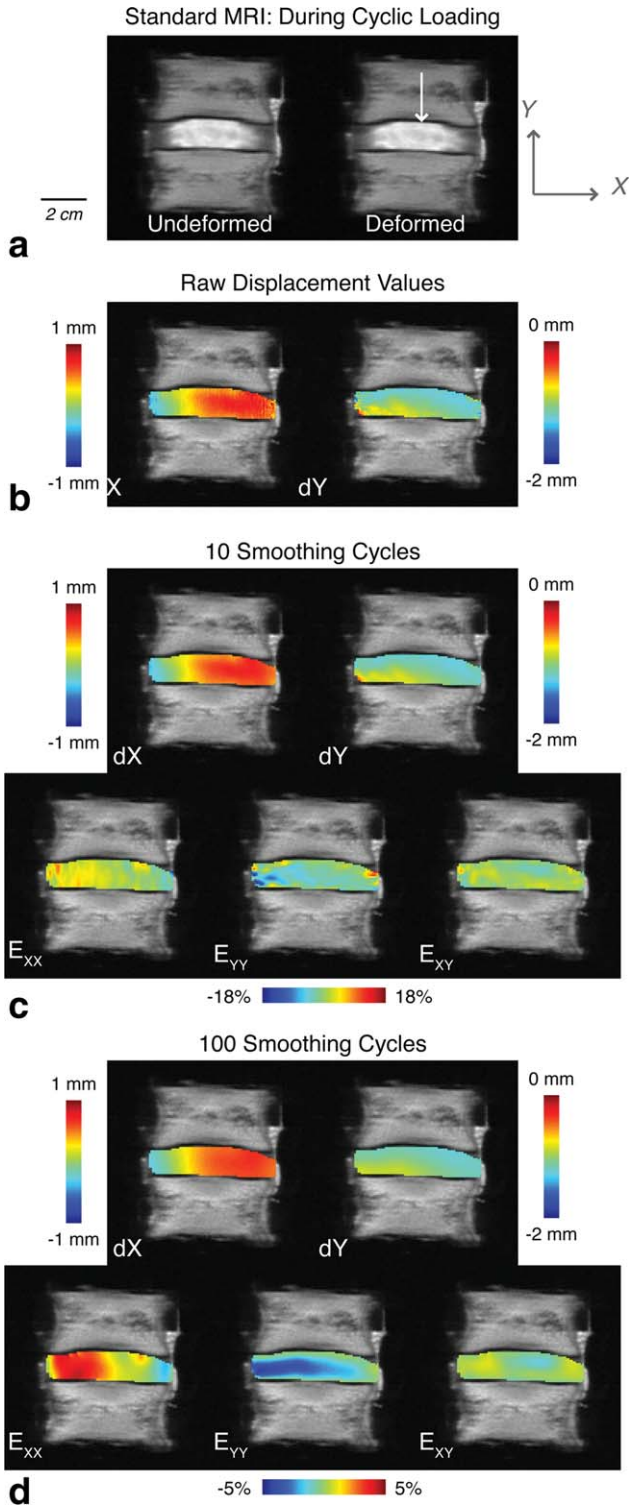

FIG. 3. Displacements and strains within an intervertebral disc during cyclic loading. Standard images of the undeformed and deformed disc during cyclic loading (**a**). Raw displacements (**b**), smoothed displacements and strains after 10 smoothing cycles (**c**) and after 100 smoothing cycles (**d**), with respect to the loading direction (*y*) and direction transverse to loading (*x*), were measured using dualMRI.

of displacement and strain values between displacement-encoded imaging and tracking of markers embedded in the silicone gel phantom. Although it is important to

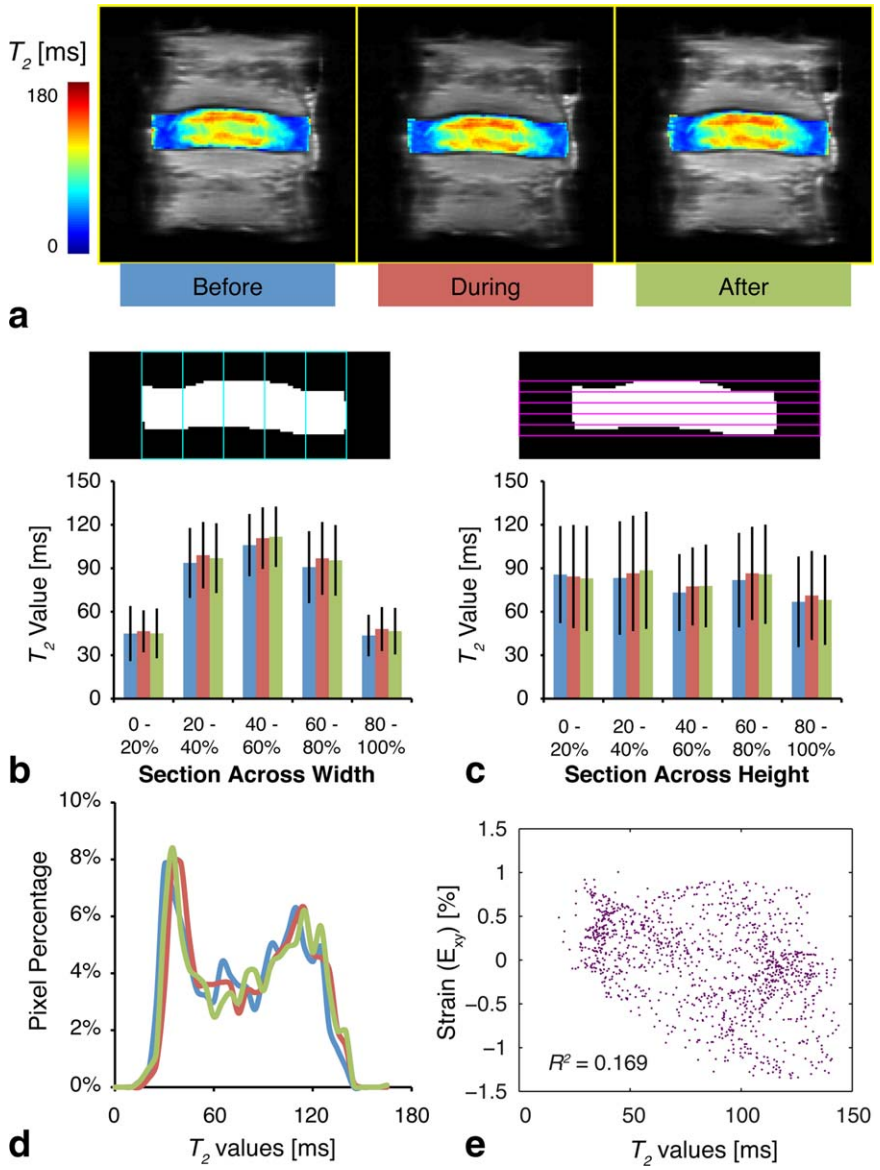

FIG. 4. T_2 analysis of a cyclically loaded intervertebral disc. T_2 maps were estimated for an intervertebral disc (**a**), before (blue), during (red), and after (green) cyclic loading in the same imaging slice as was used for dualMRI. ROIs (mask for disc before loading shown) were divided into five regions along the width (**b**) and the height (**c**) and used to compare average regional T_2 and a histogram of T_2 values (binned in 5-ms intervals) across the full disc (**d**). Although no displacements and strains were significantly correlated to T_2 values ($P > 0.05$), the relationship with E_{xy} after 100 cycles of smoothing for each pixel within the ROI is shown (**e**) because it had the highest R^2 of all linear regressions.

note that increasing the amount of smoothing could increase bias between the smoothed value and the true value, previous studies with displacement smoothing showed that this bias is often smaller than the precision (11). This validation study therefore shows that, if larger voxel sizes are acceptable for the tissue of interest, displacement precisions of better than half the spatial resolution can be achieved without smoothing, and smoothing can improve displacement and strain precisions up to 24 μm and 0.3%, respectively. Although some spatial resolution may be lost in the translation from research to clinical scanner, the ability to measure displacements and strains noninvasively in larger volumes and potentially living subjects far outweigh the disadvantages of the clinical system.

Several of the imaging parameters used in this study were limited by the imaging system, loading device, or image processing software. The effect on SNR by T_2 decay with TE (in fast spin echo acquisitions) and by T_1 decay with TM (in stimulated echo applications) are well known physical phenomena (3,4,10). Accordingly, image acquisition parameters were chosen to minimize TE and TM within the limitations of the chosen acquisition size and the timing of the load system, respectively. The displacement encoding of 0.33 π/mm was selected to avoid excessive phase wrapping and ease computational efforts in unwrapping the phase. Based on pilot studies, we expected internal deformations of no more than 3 mm in absolute value and therefore set the displacement encoding to encode 3 mm as π. Spatial resolution in this study was limited by the field of view and the choice in acquisition matrix size. In preliminary studies, we compared displacement precision for square matrix sizes of 256 × 256, 384 × 384, and 512 × 512. The additional lines of acquisition resulted in longer effective TEs and required longer load plateaus to accommodate the longer total acquisition time, resulting in attenuation of signal and loss of precision. Although a smaller matrix size (i.e., 128 × 128) could have been chosen for higher SNR and potentially improved

displacement precision, we desired a spatial resolution of at least 1 mm and therefore chose 256 × 256 acquisition matrix. Although the aforementioned parameters are limited by the current system, a detailed, parameterized study of the effects of TE, TM, displacement encoding strength, spatial resolution, and other imaging parameters could be useful in further characterizing this technique.

In this study, dualMRI was demonstrated on the clinical MRI system with a clinically relevant human intervertebral disc segment (Fig. 3). Displacement values were obtained for every pixel in the ROI using phase contrast MRI, an advantage over techniques that measure the overall change in disc height, area, or volume (17). In this study, compression of 0.7 mm and total bulging of 0.7 mm was measured from images taken during cyclic loading. These measures confirm the displacements measured at pixels on the edges of the disc with dualMRI, but dualMRI also provides internal displacements for strain calculation. In addition to the inherent material properties of the disc, the measured mechanical behavior can also be influenced by the geometry of the specimen and the loading conditions. In this case, the strains are higher on one side of the disc than the other, perhaps indicating that, under compression, the nucleus shifted to one side. This would indicate that although the entire motion segment (i.e., superior and inferior vertebral bodies with intersecting disc) was compressed axially, the geometry of the disc, including the shape and orientation of the cartilage endplates, could have caused a bending moment within the disc itself.

In previous studies, texture correlation has also been used with magnitude-based MRI to measure the internal strain of intervertebral discs (18). This previous study reported a displacement resolution of 1/20th of a pixel or 12 μm after interpolation and smoothing; however, the optimal subset of 61 pixels, equivalent to 5.2 mm in their study, reportedly resulted in loss of local strain detail. Compared to the cyclic loading conditions used in this study for dualMRI, the texture correlation study used a statically loaded disc. Although texture correlation can provide accurate strain measures in tissues that provide enough SNR and texture in magnitude images, phase-contrast techniques, including dualMRI, do not depend on image texture, which is especially an advantage in tissues that tend toward spatial homogeneity in MRI signal intensity.

In this study, we also measured T_2 before, during, and after cyclic loading with the goal of directly comparing T_2 and displacements and strains during cyclic loading (Fig. 4). In cartilage, T_2 values are correlated to collagen content and orientation (19) and are related to mechanical properties measured in extracted tissue (20). T_2 values also significantly decrease with degeneration in the disc (21,22), so a relationship between T_2 values and the mechanical behavior of the disc would not be unexpected. Within this single specimen, there was no apparent difference in overall T_2 values or distribution between the three loading conditions and no correlation between T_2 under cyclic loading and dualMRI measures of mechanical behavior. Further study with an increased number of specimens would be required to show any significant changes in T_2 during cyclic loading and to show generalized relationships between T_2 and mechanical behavior. Although a recent study showed no change in T_1 and T_2 with static compression and subsequent relaxation (23), a study that compares T_2 before, during and after cyclic loading may better represent physiological activities including walking and could elucidate biochemical changes during cyclic loading. The T_2 values of the disc fall on the higher end of the range found in human intervertebral discs, although most of the discs examined in a previous study were degenerated at various levels (15,24). Although it would be amiss to form any conclusions based on a single specimen, it is nonetheless important to point out that complementing both standard MRI and quantitative MRI techniques with dualMRI, which has the ability to noninvasively assess mechanical behavior, enables a more thorough understanding of the interplay between structure, biochemistry, and mechanical function in a variety of tissues and biomaterials.

Although this study presents promising results for displacement and strain precision, there are a number of improvements that can expedite implementation in vivo. The use of surface array coils should be considered for tissues that would be inappropriate for a volume coil, with SNR as a key deciding factor. Although SSFSE is a fast sequence, it is limited in terms of spatial resolution and relies on the assumption of k-space symmetry to "fill" the remainder of k-space in post processing. A number of acquisition sequences could be substituted for SSFSE, although each acquisition technique presents its own advantages and disadvantages. Additionally, as a technique that synchronizes displacement-encoded MRI with externally applied loading, dualMRI requires an MRI-compatible loading system that can consistently load the tissue or tissues of interest in the confines of a clinical MRI system. The loading system should be able to bring the tissue of interest to a quasi-steady state load-deformation response (13) to achieve optimal image quality. Mechanically loading parts of a living animal or human volunteer, without inducing unwanted motion artifacts or causing undue discomfort, poses a strong technical challenge. Although there are a number of developments that remain to be surmounted, this study nonetheless demonstrates for the first time the use of dualMRI on a clinical MRI system, establishing the in vivo potential.

CONCLUSIONS

dualMRI was translated to a clinical 3T MRI system for the precise measurement of internal tissue deformation. The precision of displacement measurements was below half the spatial resolution of the image acquisition. Strain precisions were below 2% after just 10 smoothing cycles, and more smoothing (i.e., 100 smoothing cycles) permitted strain precisions of 0.3%. The sequence was demonstrated with a controlled loading system, permitting the visualization of displacement and strain fields in a cyclically compressed intervertebral disc. T_2 mapping during cyclic loading also provided an indication of the structural and biochemical characteristics of the disc. A combination of dualMRI and quantitative MRI could

be used in combination to gain insight into the structure and mechanical function of tissue noninvasively.

ACKNOWLEDGMENTS

The authors gratefully acknowledge the assistance of Kent Butz and Paull Gossett, in the specimen preparation and the design of the loading apparatus, Aaditya Chandramouli for his assistance in specimen preparation, Gregory Tamer for his technical assistance on the clinical MRI system, and Eric Nauman for advice and access to the cadaveric specimen.

REFERENCES

1. Nguyen AM, Johannessen W, Yoder JH, Wheaton AJ, Vresilovic EJ, Borthakur A, Elliott DM. Noninvasive quantification of human nucleus pulposus pressure with use of T1rho-weighted magnetic resonance imaging. J Bone Joint Surg Am 2008;90:796–802.
2. Nissi MJ, Rieppo J, Toyras J, Laasanen MS, Kiviranta I, Nieminen MT, Jurvelin JS. Estimation of mechanical properties of articular cartilage with MRI—dGEMRIC, T2 and T1 imaging in different species with variable stages of maturation. Osteoarthritis Cartilage 2007;15: 1141–1148.
3. Neu CP, Walton JH. Displacement encoding for the measurement of cartilage deformation. Magn Reson Med 2008;59:149–155.
4. Chan DD, Neu CP. Transient and microscale deformations and strains measured under exogenous loading by noninvasive magnetic resonance. PLoS One 2012;7:e33463.
5. Chan DD, Neu CP, Hull ML. Articular cartilage deformation determined in an intact tibiofemoral joint by displacement-encoded imaging. Magn Reson Med 2009;61:989–993.
6. Chan DD, Khan SN, Ye XJ, Curtiss SB, Gupta MC, Klineberg EO, Neu CP. Mechanical deformation and glycosaminoglycan content changes in a rabbit annular puncture disc degeneration model. Spine 2011;36:1438–1445.
7. Axel L, Dougherty L. Heart wall motion: Improved method of spatial modulation of magnetization for MR imaging. Radiology 1989;172: 349–350.
8. Epstein FH, Gilson WD. Displacement-encoded cardiac MRI using cosine and sine modulation to eliminate (CANSEL) artifact-generating echoes. Magn Reson Med 2004;52:774–781.
9. Bernstein MA, Grgic M, Brosnan TJ, Pelc NJ. Reconstructions of phase contrast, phased array multicoil data. Magn Reson Med 1994;32:330–334.
10. Aletras AH, Ding S, Balaban RS, Wen H. DENSE: Displacement encoding with stimulated echoes in cardiac functional MRI. J Magn Reson 1999;137:247–252.
11. Chan DD, Toribio D, Neu CP. Displacement smoothing for the precise MRI-based measurement of strain in soft biological tissues. Comput Methods Biomech Biomed Eng 2013;16:852–860.
12. Geers MGD, de Borst R, Brekelmans WAM. Computing strain fields from discrete displacement fields in 2D-solids. Int J Solids Struct 1996;33:4293–4307.
13. Martin KJ, Neu CP, Hull ML. Quasi-steady-state displacement response of whole human cadaveric knees in a MRI scanner. J Biomech Eng 2009;131:081004.
14. Marinelli NL, Haughton VM, Munoz A, Anderson PA. T2 relaxation times of intervertebral disc tissue correlated with water content and proteoglycan content. Spine (Phila Pa 1976) 2009;34:520–524.
15. Marinelli NL, Haughton VM, Anderson PA. T2 relaxation times correlated with stage of lumbar intervertebral disk degeneration and patient age. AJNR Am J Neuroradiol 2010;31:1278–1282.
16. Jenkins JP, Stehling M, Sivewright G, Hickey DS, Hillier VF, Isherwood I. Quantitative magnetic resonance imaging of vertebral bodies: A T1 and T2 study. Magn Reson Imaging 1989;7:17–23.
17. Race A, Broom ND, Robertson P. Effect of loading rate and hydration on the mechanical properties of the disc. Spine (Phila Pa 1976) 2000;25:662–669.
18. O'Connell GD, Johannessen W, Vresilovic EJ, Elliott DM. Human internal disc strains in axial compression measured noninvasively using magnetic resonance imaging. Spine 2007;32:2860–2868.
19. Xia Y, Moody JB, Alhadlaq H. Orientational dependence of T2 relaxation in articular cartilage: A microscopic MRI (microMRI) study. Magn Reson Med 2002;48:460–469.
20. Wayne JS, Kraft KA, Shields KJ, Yin C, Owen JR, Disler DG. MR imaging of normal and matrix-depleted cartilage: Correlation with biomechanical function and biochemical composition. Radiology 2003;228:493–499.
21. Antoniou J, Pike GB, Steffen T, Baramki H, Poole AR, Aebi M, Alini M. Quantitative magnetic resonance imaging in the assessment of degenerative disc disease. Magn Reson Med 1998;40:900–907.
22. Zhang H, Yang S, Wang L, Park P, La Marca F, Hollister SJ, Lin CY. Time course investigation of intervertebral disc degeneration produced by needle-stab injury of the rat caudal spine: Laboratory investigation. J Neurosurg Spine 2011;15:404–413.
23. Manac'h YG, Perie D, Gilbert G, Beaudoin G. Sensitivity of multiparametric MRI to the compressive state of the isolated intervertebral discs. Magn Reson Imaging 2013;31:36–43.
24. Takashima H, Takebayashi T, Yoshimoto M, Terashima Y, Tsuda H, Ida K, Yamashita T. Correlation between T2 relaxation time and intervertebral disk degeneration. Skeletal Radiol 2012;41:163–167.

Journal of Biomechanics 47 (2014) 2801–2806

Contents lists available at ScienceDirect

Journal of Biomechanics

journal homepage: www.elsevier.com/locate/jbiomech
www.JBiomech.com

Short Communication

Comparison of intervertebral disc displacements measured under applied loading with MRI at 3.0 T and 9.4 T☆

Deva D. Chan [a], Paull C. Gossett [a], Kent D. Butz [b], Eric A. Nauman [a,b], Corey P. Neu [a,*]

[a] Weldon School of Biomedical Engineering, Purdue University, West Lafayette, IN, USA
[b] School of Mechanical Engineering, Purdue University, West Lafayette, IN, USA

ARTICLE INFO

Article history:
Accepted 30 May 2014

Keywords:
Displacement-encoded imaging
High-field MRI
Clinical MRI
Biomechanics
Elastography

ABSTRACT

The purpose of this study was to compare displacement behavior of cyclically loaded cadaveric human intervertebral discs as measured noninvasively on a clinical 3.0 T and a research 9.4 T MRI system. Intervertebral discs were cyclically compressed at physiologically relevant levels with the same MRI-compatible loading device in the clinical and research systems. Displacement-encoded imaging was synchronized to cyclic loading to measure displacements under applied loading with MRI (dualMRI). Displacements from the two systems were compared individually using linear regression and, across all specimens, using Bland–Altman analysis. In-plane displacement patterns measured at 3.0 T and 9.4 T were qualitatively comparable and well correlated. Bland–Altman analyses showed that over 90% of displacement values within the intervertebral disc regions of interest lay within the limits of agreement. Measurement of displacement using dualMRI using a 3.0 T clinical system is comparable to that of a 9.4 T research system. Additional refinements of software, technique implementation, and image processing have potential to improve agreement between different MRI systems. Despite differences in MRI systems in this initial implementation, this work demonstrates that dualMRI can be reliably implemented at multiple magnetic field strengths, permitting translation of dualMRI for a variety of applications in the study of tissue and biomaterial biomechanics.

1. Introduction

The mechanical behavior is closely linked to tissue form and function, particularly in tissues whose primary physiological role is the support of load. As a noninvasive imaging modality, magnetic resonance imaging (MRI) has the capability of measuring not only the morphology but also the biomechanics of tissues in their native mechanical environment (Glaser et al., 2006; Neu and Walton, 2008; Zhong et al., 2010). Noninvasive measurement of displacements under applied loading with MRI (dualMRI) can be implemented on both clinical and high-field research MRI systems (Chan and Neu, 2012, 2013). dualMRI involves the synchronization of cyclic loading, which is applied by an MRI-compatible loading device, with displacement-encoded MRI. Numerous factors influence the MRI-based measurement of displacements in biomaterials and tissues, including the magnitude and frequency of cyclic loading, the geometry and configuration of the physical environment, and inherent material properties of the tissue, which is often viscoelastic and heterogeneous (Neu and Walton, 2008; Chan et al., 2009, 2011).

Conversely, the MRI acquisition technique and parameters, the software and hardware limitations on different MRI systems, and the signal and contrast of the image could also affect the measurement of displacements. The precision of the displacement-encoded MRI sequences used with dualMRI is already known to depend on the signal-to-noise ratio and also on the strength of the encoding gradient (Chan and Neu, 2012). Knowledge of how displacements measured on a clinical MRI system compare to those measured on a higher field research system would be of vital importance to the translation of dualMRI applications to clinical use. Therefore, the goal of this study was to compare displacements measured in a cyclically loaded intervertebral disc by dualMRI on a high-field (9.4 Tesla (T)) research MRI system to those measured on a 3.0 T clinical system under the same loads.

2. Methods

Fresh-frozen human cadaveric lumbar spines ($n=3$) were obtained from an organ and tissue donation center (Unyts, Buffalo, NY) and thawed on ice prior to dissection. Motion segments consisting of the 4th and 5th lumbar vertebral bodies and the intervertebral disc were isolated and then potted with a fiberglass resin to

☆**Grant support:** NSF CMMI 1100554, NIH R25 EB013029-02, NIH S10 RR019920-01, NIH R01 AR063712, NIH R21 AR064178, and Indiana CTSI Core Pilot Funding.

* Correspondence to: 206 South Martin Jischke Drive, West Lafayette, IN 47907, USA. Tel.: +1 765 496 1426; fax: +1 765 494 0902.
E-mail address: cpneu@purdue.edu (C.P. Neu).

http://dx.doi.org/10.1016/j.jbiomech.2014.05.026
0021-9290/

be secured in a custom MRI-compatible cyclic loading device. The device permitted cyclic axial compression of the disc at 445 N in the superior-to-inferior direction. Load was applied for 1.5 s and then fully released to permit tissue recovery, every 3 s, during the preconditioning period and when synchronized with imaging as described below. The discs were wrapped in PBS-soaked gauze to prevent desiccation of the disc during experiments.

Displacements were measured within the human intervertebral discs by dualMRI on a 9.4 T Bruker Biospec system (Bruker Medical GMBH, Ettlington, Germany). The discs were cyclically loaded, and, for each disc, dualMRI did not commence until a steady state load-displacement response was achieved. dualMRI data was acquired using displacement encoding with stimulated echoes (DENSE) and a true fast imaging under steady-state precession (TrueFISP) sequence. Key acquisition parameters were as follows: echo time (TE)=1.6 ms, field of view (FOV)=64 mm × 64 mm, spatial resolution=234 μm × 234 μm, and slice thickness=2 mm. Displacements were encoded at 0.32 rad/mm. After imaging, discs were frozen at −20 °C and later thawed at 4 °C for the 3.0 T experiments.

On the other hand, displacements were measured on a 3.0 T clinical MRI system (General Electric Signa HDx, Waukesha, WI) using displacement encoding with a single-shot fast spin echo (SSFSE) acquisition. Load parameters were identical to those described previously, and SSFSE acquisition parameters were TE=62 ms, FOV=180 mm × 180 mm, spatial resolution=703 μm × 703 μm, slice thickness=3 mm, and displacements were encoded at 0.14 rad/mm. Raw displacements from either system were not smoothed prior to the following data analyses; however, because smoothing improves the precision of the displacement measurement (Chan et al., 2012), the variance in raw displacement measurements represent a conservative comparison between the two systems.

Regions of interest (ROIs) were manually selected for each specimen and each MRI system. The selection of the ROI on the lower resolution images (3.0 T data) was performed independently of the ROI selection in data from the 9.4 T system. Imaged volumes from the 9.4 T and 3.0 T experiments were manually registered to the same specimen-based coordinate system to permit comparison. The size of the higher resolution 9.4 T image was expanded to replicate the same FOV as the 3.0 T data and then resized with bicubic interpolation to reduce the spatial resolution, generating an image with the same size (256 × 256 pixels) as the 3.0 T image. The same image expansion and interpolation was performed for the displacement maps and ROIs for each specimen. Only points that lay within both the 3.0 T intervertebral disc ROI and the reshaped 9.4 T ROI were chosen for analysis to eliminate differences resulting from the manual ROI selection and the interpolation process. Displacements in the x (transverse to loading) and y (aligned with loading) directions were compared with a linear regression within each specimen. A Bland–Altman analysis was also performed, with the limits of agreement defined as the bias (i.e., average difference) ± 1.96 × the standard deviation of the differences (Bland and Altman, 1986).

3. Results

The signal-to-noise ratios of the disc regions of interest in the displacement-encoded images were comparable at 11.13 ± 4.61 and 11.15 ± 2.50 on the 9.4 T and 3.0 T systems, respectively. Displacements in x and y (dx and dy) measured at 9.4 T qualitatively showed similar patterns to those measured at 3.0 T (Fig. 1). Linear regressions between dx on the 9.4 T and dx on the 3.0 T showed agreement ranging R^2=0.66–0.85, and a similar analysis between the 9.4 T and 3.0 T dy values resulted in R^2=0.39–0.82 (Fig. 2). The standard deviation of differences in displacements ranged from 0.21 to 0.26 mm in x and from 0.13 to 0.22 mm in y in individual discs, with limits of agreement defined as 1.96 times that standard deviation (Table 1). The combined disc analysis resulted in a standard deviation of 0.52 mm for dx and 0.27 mm for dy. Bland–Altman analyses within each specimen showed that a majority (i.e. a range from 92.9% to 96.5%) of displacement values were within the limits of agreement (Fig. 3). After grouping all specimens, Bland–Altman analysis showed that 93.4% and 94.1% of dx and dy values agreed (Fig. 4). However, the mean differences between dx and dy values of the 3.0 T and the 9.4 T measurements across all specimens were 0.12 and 0.26 mm, respectively, which were comparable or less than the image pixel dimensions acquired at 9.4 T.

4. Discussion

This study demonstrates similar displacements measured at two different field strengths using dualMRI in the intervertebral disc. Previous studies of intervertebral disc mechanics have used various MRI techniques to compute internal strains via digital image correlation (Gilchrist et al., 2004; O'Connell et al., 2007), tissue stiffness via MR elastography (Cortes et al., 2013), and material properties via correlations to quantitative MRI biomarkers (Antoniou et al., 2013).

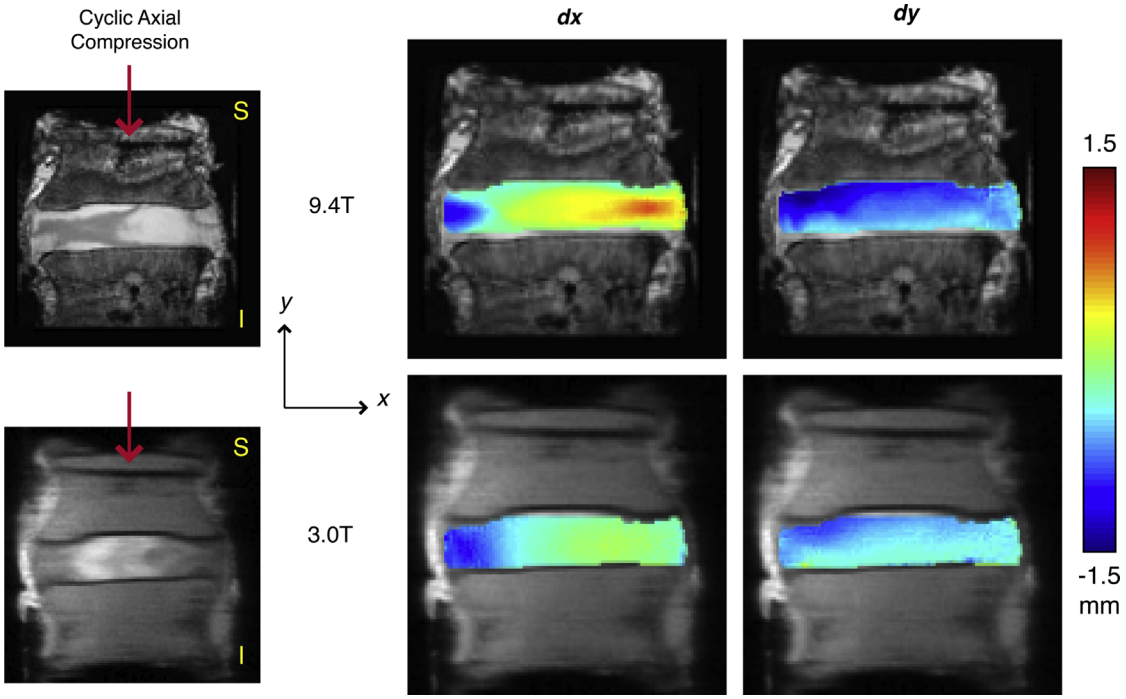

Fig. 1. Displacements measured on research (9.4 T) and clinical (3.0 T) MRI systems under applied loading. Cyclic compression was applied using an MRI-compatible apparatus along the superior-to-inferior axis of cadaveric human intervertebral discs. In-plane displacements were measured in the coronal plane through the widest part of the intervertebral disc in the direction of loading (y) and the direction transverse to loading (x). The high spatial resolution of the 9.4 T images, shown here before adjustments were made to match the spatial resolution of the 3.0 T acquisition, permits a better representation of the spatial variations in displacements within the disc, as well as a broader range of displacement values.

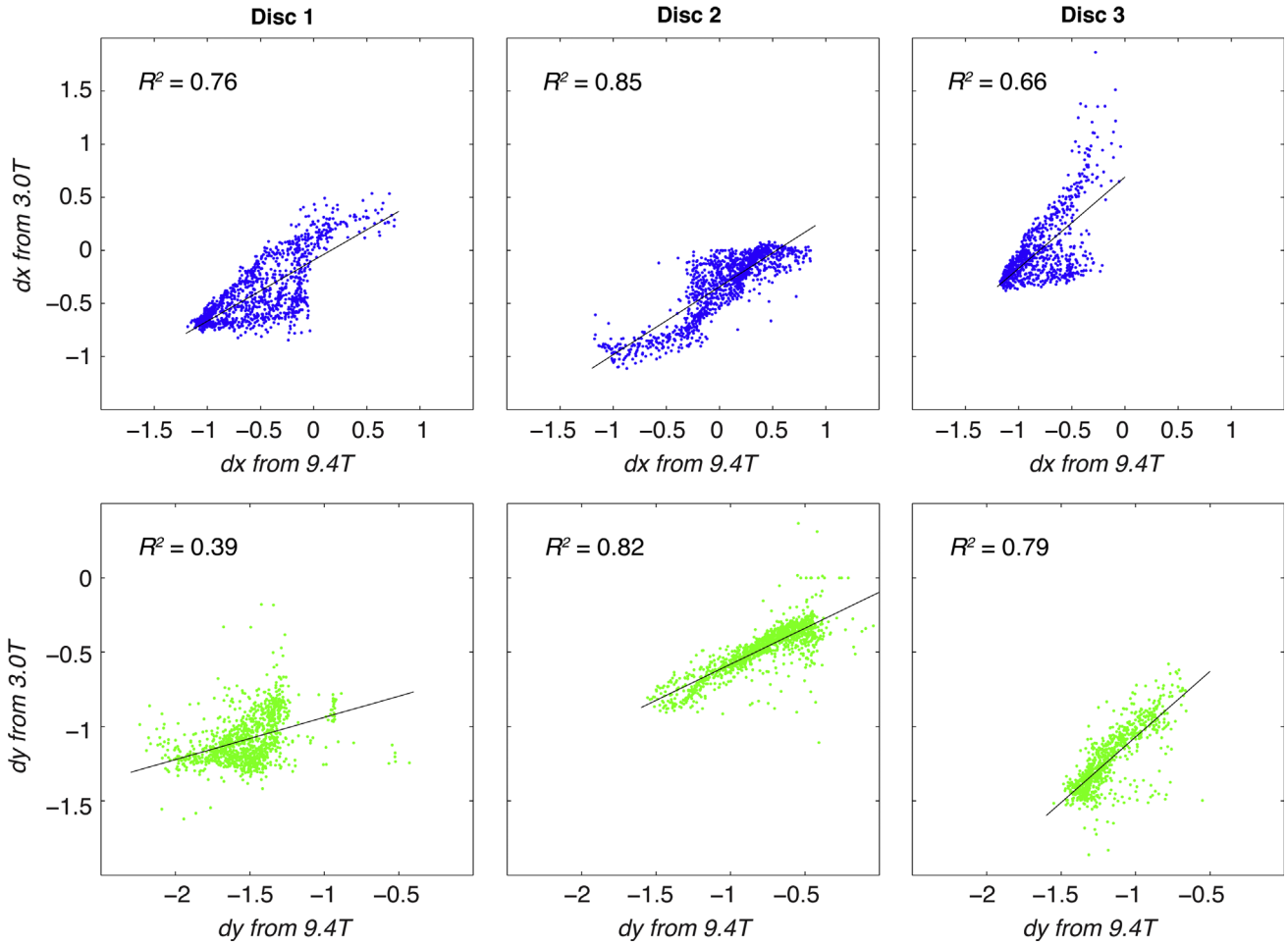

Fig. 2. Linear regression comparisons of displacements measured at 9.4 and 3.0 T in individual discs. Displacements in *x* and *y* were measured during axial compression and compared for each overlapping point in regions of interest for each of three disc specimens. In order to encompass all sources of variability in the systems, displacements were not smoothed prior to this comparison. Correlation coefficients (R^2) varied from 0.39 to 0.85. Despite numerous sources of differences between the MRI systems (e.g. voxel size) and set up (e.g. specimen positioning), agreement in the correlation coefficient data was observed, with additional analysis presented in Fig. 3.

Table 1
Mean difference and limits of agreement (as defined as 1.96 times the standard deviation) of displacements in the loading (*y*) and transverse (*x*) directions were calculated based on a Bland–Altman analysis of the individual specimens and the combined data.

	Displacement direction	Lower limit of agreement [mm]	Mean difference [mm]	Upper limit of agreement [mm]
Disc 1	*x*	−0.40	0.12	0.64
	y	0.00	0.44	0.88
Disc 2	*x*	−0.77	−0.36	0.06
	y	−0.02	0.31	0.64
Disc 3	*x*	0.31	0.80	1.30
	y	−0.30	−0.05	0.20
Combined data	*x*	−0.90	0.12	1.13
	y	−0.26	0.26	0.78

These and similar MRI-related techniques have also been applied to a variety of other biomechanically relevant soft tissue systems (Herberhold et al., 1999; Hardy et al., 2005; Subburaj et al., 2012).

As expected, displacements within the intervertebral discs reflected both the material properties and the specific loading environment. Qualitative comparison of the displacement fields shows that the bulging of the disc, as evidenced by the *dx* fields, was consistent under the same cyclic axial compression. The *dy* fields also showed a greater displacement on one side of the disc than the other, in response to axial compression. However, the displacements measured at 3.0 T appeared more diffuse, possibly because of the lower initial spatial resolution at that field.

In comparing the displacement fields measured at 3.0 and 9.4 T, differences in *dx* and *dy* can be attributable to the use of two inherently different hardware and software systems, biological variations, and other factors, all of which are discussed further below. The linear correlation analysis shows a varying degree of correspondence between displacements at 3.0 and 9.4 T (R^2=0.39–0.85, Fig. 2). Although this analysis is based on a paired design, it is important to note that a number of factors that can

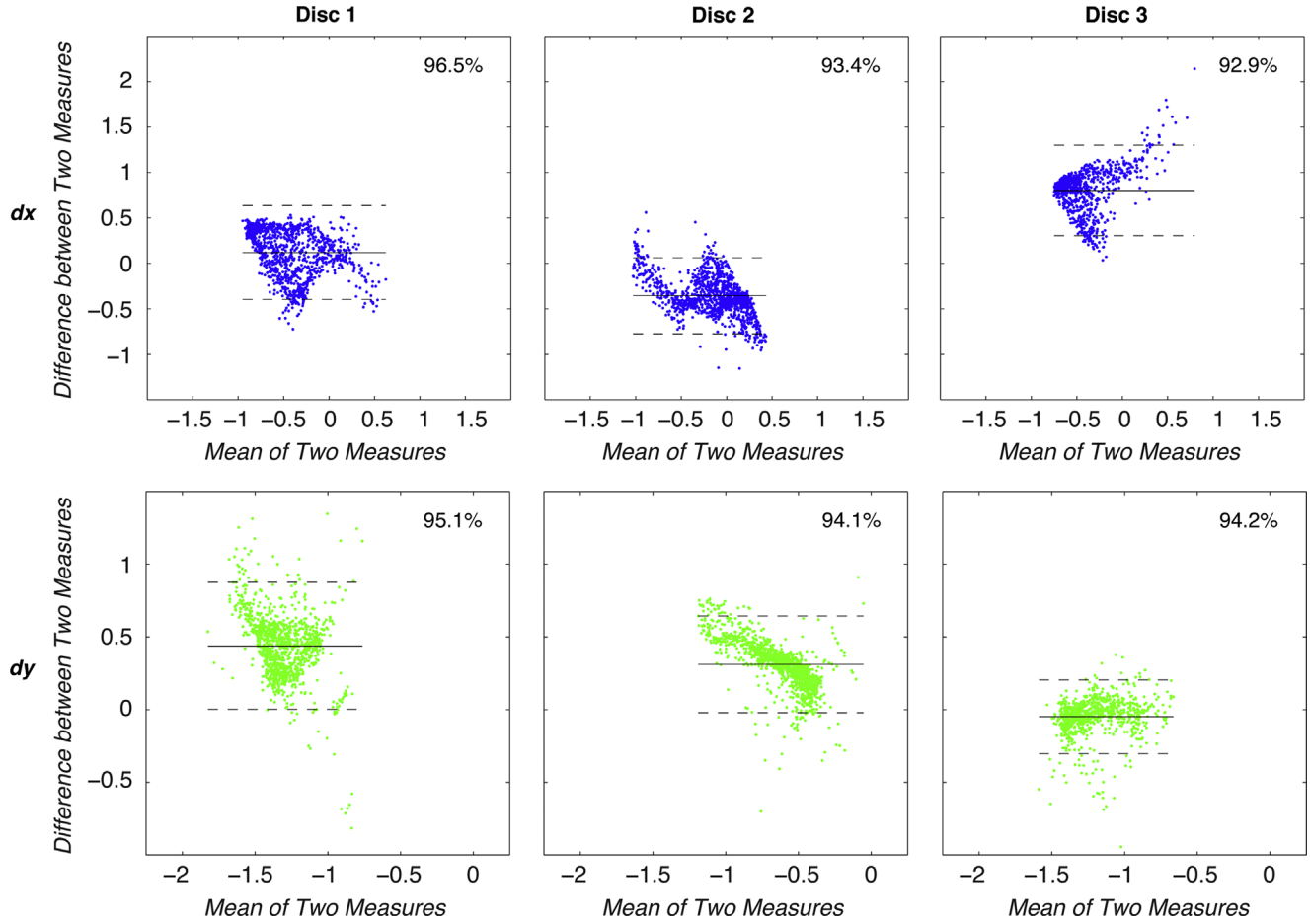

Fig. 3. Bland–Altman analyses were performed to compare displacements measured at 9.4 T and 3.0 T in individual discs. For each point, the mean of and the difference between displacements in *x* and *y* were plotted to visualize the agreement between the two systems. Between 92.9% and 96.5% of the points of interest fall within the limits of agreement, as listed in Table 1.

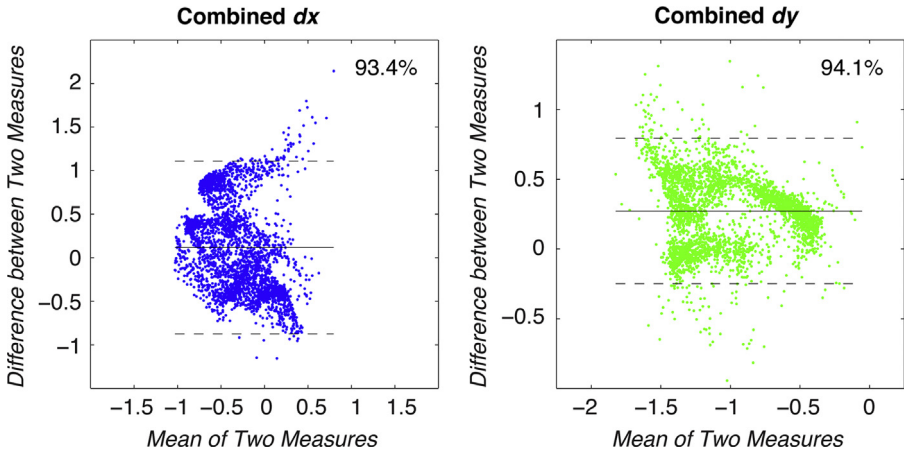

Fig. 4. Bland–Altman analysis was performed to compare displacements measured in all discs. Taking the values for all points of interest across all the discs, the mean and difference between *x* and *y* displacements were calculated and compared. Values for *dx* and *dy* showed that 93.4% and 94.1% of displacement values lay within the limits of agreement, with standard deviations of 0.52 and 0.27 mm, respectively.

affect differences in displacements may not be linear. These include spatial inhomogeneities of the main and gradient magnetic fields, biological variability both between discs and within the same disc after time and handling, and differences in the mechanical systems. Although a multi-factored analysis of variance could also be performed to test several of these factors, that experimental design is challenging in part due to the limited lifespan of biological specimen during repeated testing and the cost-prohibitive imaging time required on MRI systems.

Despite the range of coefficients of variation in the linear analysis, the 3.0 T data showed good agreement with the displacements measured at 9.4 T under a Bland–Altman analysis (Fig. 3),

a method that quantifies the agreement between two different measurement techniques without assumptions of linear correlation (Bland and Altman, 1986). The measurement of the difference between displacement values at each point also permitted displacements across all specimens to be compared between 3.0 T and 9.4 T with a pooled Bland–Altman analysis (Fig. 4), which takes into account the differences between field strengths in all the specimens. Therefore, the variability in difference values inherent to biological variability (between different discs) and repeatability of the mechanics (within the same disc) are also included in the limits of agreement of the pooled analysis, in addition to differences inherent to the imaging itself.

Interestingly, the Bland–Altman analysis showed that the mean difference between the two systems in both *dx* and *dy* were non-zero. Because the pulse sequence and image processing for both systems must balance the encoding and un-encoding actions, in theory there should be no difference in displacement values due to the imaging systems. However, in practice, MRI systems have their unique technical limitations, so displacement measurements on the two systems can be biased by inhomogeneities in the magnetic field, imperfect gradient timings, and other hardware limitations that affect the generation and measurement of signal phase. To remedy this within each system, a separate no-load calibration scan can be performed with the specimen prior to any loading to aid in removing any sample-specific and location-dependent bias during image processing. However, this essentially doubles the total scan time, leaving a no-load calibration scan of a non-moving imaging phantom as a faster, but possibly less effective, method of reducing system-specific biases.

Because the method of filtering can have an effect on the precision of the displacement measurements (Chan et al., 2012), only the raw displacements, before any smoothing, were examined in this study. We have previously shown that displacement precision also depends on the SNR (Neu et al., 2005; Chan et al., 2012), and image parameters permitted a similar SNR between both systems for this study. Increases in SNR on both systems would presumably improve the correlations and agreement measures. While it would be ideal to vary only the strength of the main magnetic field, there were also differences in the strength of the encoding gradient, the acquisition sequence used to measure displacement-encoded data, and the spatial resolution due to the software and hardware limitations of the two systems in this study. For example, the selection of the imaging slice was based on visualizing landmarks, and the resulting images do not depict identical disc morphologies, especially considering that imaging parameters limit the 3.0 T system to 3-mm thick, and 18-mm wide slices. Nonetheless, in the typical circumstances that these displacement data would be used, displacement fields would be smoothed within the regions of interest (Chan et al., 2012) prior to calculations of strain. Although the smoothing parameters would be chosen based on spatial resolution as well as the geometry of the region of interest, the difference between equivalent displacement-encoded images from two different systems would be expected to be no worse than the raw displacement (i.e. without smoothing) condition.

Another consideration in this study, as mentioned above, is the difference in the loading environment between the 9.4 T and 3.0 T systems. Indeed, the design of a loading apparatus is specific to the desired mechanism, in this case axial compression, as well as constrained by the interface with the imaging hardware. On the 9.4 T system, the loading device is supported by a manual gantry and secured to the MRI system with positioning screws. On the 3.0 T system which is designed primarily for patient use, the loading apparatus was placed on the automatic gantry with supports underneath to hold its position. However, there was no physical attachment of the loading apparatus to the clinical MRI system, so slight variations in the alignment and orientation of the apparatus, which includes the specimen, to the coordinate system of the magnet are also possible. In addition, there may be variations due to the replacement of the potted disc in the loading apparatus for the 3.0 T study after it was removed for storage following the 9.4 T experiments. An extra freeze-thaw cycle, which was a logistical necessity between experiments, could also have affected the mechanical properties of the disc itself, since freezing is known to affect characterization of cartilage mechanics (Willett et al., 2005). The transport and storage of the discs between testing could also have affected the hydration state of the discs, which would in turn alter their mechanical behavior under compression, though care was taken to minimize hydration state changes through the use of PBS-soaked gauze that completely wrapped the exposed areas of the discs.

Further studies could eliminate the potential for mechanical differences that occur with time, degradation, and storage by using non-biological (e.g. silicone gel) materials. However, few non-biological materials share the viscoelastic and heterogeneous behavior of biomaterials and tissues, potentially limiting the usefulness of such a comparison between systems.

In conclusion, despite inherent differences in 9.4 T and 3.0 T MRI systems, displacements measured at the two magnetic field strengths correspond qualitatively and quantitatively, according to Bland–Altman analysis. Further research should focus on using a non-biologic material for comparisons and endeavor to reproduce as many of the same hardware, software, and imaging parameters as possible on the compared systems. Additionally, it is important to note that for every new loading apparatus design, differing software implementation, or MRI system, an analysis of internal consistency should be performed to assess displacement bias and precision, in addition to comparisons with previously validated systems. Nonetheless, the results of this study indicate promise that displacements and strains measured on a clinical 3.0 T MRI system can be used to characterize mechanical behavior with dualMRI. Translation of dualMRI from research to clinical systems could permit the visualization of the biomechanical response to various loading states, including shear and torsion, in intervertebral discs and other soft orthopedic tissues.

Conflict of interest statement

The authors have no financial or personal conflicts of interest to declare.

Acknowledgments

Funding for this study was provided by NSF CMMI 1100554, NIH R25 EB013029-02, NIH S10 RR019920-01, NIH R01 AR063712, NIH R21 AR064178, and Indiana CTSI Core Pilot Funding. Study sponsors were not involved in the design of the study, the collection, analysis and interpretation of data, the writing of the manuscript, nor the decision to publish. The authors thank Aaditya Chandramouli for assistance with specimen preparation and also Limin Li, Gregory Tamer, and Thomas Talavage for their technical expertise on MRI systems.

References

Antoniou, J., Epure, L.M., Michalek, A.J., Grant, M.P., Iatridis, J.C., Mwale, F., 2013. Analysis of quantitative magnetic resonance imaging and biomechanical parameters on human discs with different grades of degeneration. J. Magn. Reson. Imaging.

Bland, J.M., Altman, D.G., 1986. Statistical methods for assessing agreement between two methods of clinical measurement. Lancet 1 (8476), 307–310.

Chan, D.D., Khan, S.N., Ye, X.J., Curtiss, S.B., Gupta, M.C., Klineberg, E.O., Neu, C.P., 2011. Mechanical deformation and glycosaminoglycan content changes in a rabbit annular puncture disc degeneration model. Spine 36 (18), 1438–1445.
Chan, D.D., Neu, C.P., 2012. Transient and microscale deformations and strains measured under exogenous loading by noninvasive magnetic resonance. PLoS One 7 (3), e33463.
Chan, D.D., Neu, C.P., 2013. Intervertebral disc internal deformation measured by displacements under applied loading with MRI at 3 T. Magn. Reson. Med..
Chan, D.D., Neu, C.P., Hull, M.L., 2009. in situ deformation of cartilage in cyclically loaded tibiofemoral joints by displacement-encoded MRI. Osteoarthr. Cartil. 17 (11), 1461–1468.
Chan, D.D., Toribio, D., Neu, C.P., 2012. Displacement smoothing for the precise MRI-based measurement of strain in soft biological tissues. Comput. Methods Biomech. Biomed. Eng..
Cortes, D.H., Magland, J.F., Wright, A.C., Elliott, D.M., 2013. The shear modulus of the nucleus pulposus measured using magnetic resonance elastography: a potential biomarker for intervertebral disc degeneration. Magn. Reson. Med..
Gilchrist, C.L., Xia, J.Q., Setton, L.A., Hsu, E.W., 2004. High-resolution determination of soft tissue deformations using MRI and first-order texture correlation. IEEE Trans. Med. Imaging 23 (5), 546–553.
Glaser, K.J., Felmlee, J.P., Manduca, A., Kannan Mariappan, Y., Ehman, R.L., 2006. Stiffness-weighted magnetic resonance imaging. Magn. Reson. Med. 55 (1), 59–67.
Hardy, P.A., Ridler, A.C., Chiarot, C.B., Plewes, D.B., Henkelman, R.M., 2005. Imaging articular cartilage under compression—cartilage elastography. Magn. Reson. Med. 53 (5), 1065–1073.
Herberhold, C., Faber, S., Stammberger, T., Steinlechner, M., Putz, R., Englmeier, K.H., Reiser, M., Eckstein, F., 1999. in situ measurement of articular cartilage deformation in intact femoropatellar joints under static loading. J. Biomech. 32 (12), 1287–1295.
Neu, C.P., Hull, M.L., Walton, J.H., 2005. Error optimization of a three-dimensional magnetic resonance imaging tagging-based cartilage deformation technique. Magn. Reson. Med. 54 (5), 1290–1294.
Neu, C.P., Walton, J.H., 2008. Displacement encoding for the measurement of cartilage deformation. Magn. Reson. Med. 59 (1), 149–155.
O'Connell, G.D., Johannessen, W., Vresilovic, E.J., Elliott, D.M., 2007. Human internal disc strains in axial compression measured noninvasively using magnetic resonance imaging. Spine 32 (25), 2860–2868.
Subburaj, K., Souza, R.B., Stehling, C., Wyman, B.T., Le Graverand-Gastineau, M.P., Link, T.M., Li, X., Majumdar, S., 2012. Association of MR relaxation and cartilage deformation in knee osteoarthritis. J. Orthop. Res. 30 (6), 919–926.
Willett, T.L., Whiteside, R., Wild, P.M., Wyss, U.P., Anastassiades, T., 2005. Artefacts in the mechanical characterization of porcine articular cartilage due to freezing. Proc. Inst. Mech. Eng. [H] 219 (1), 23–29.
Zhong, X., Spottiswoode, B.S., Meyer, C.H., Kramer, C.M., Epstein, F.H., 2010. Imaging three-dimensional myocardial mechanics using navigator-gated volumetric spiral cine DENSE MRI. Magn. Reson. Med. 64 (4), 1089–1097.